Site-resolved imaging of a bosonic Mott insulator using ytterbium atoms

Martin Miranda,[*] Ryotaro Inoue, Naoki Tambo, and Mikio Kozuma

Department of Physics, Tokyo Institute of Technology, 2-12-1 O-okayama, Meguro-ku, Tokyo 152-8550, Japan

(Received 24 April 2017; published 25 October 2017)

We demonstrate site-resolved imaging of a strongly correlated quantum system without relying on laser cooling techniques during fluorescence imaging. We observe the formation of Mott shells in the insulating regime and realize thermometry in an atomic cloud. This work proves the feasibility of the noncooled approach and opens the door to extending the detection technology to new atomic species.

I. INTRODUCTION

Since the creation of site-resolved fluorescence-imaging devices capable of observing a quantum gas trapped in a two-dimensional optical lattice [1], there has been tremendous progress in the study of strongly correlated quantum systems. By observing the superfluid-to-Mott-insulator transition at the single atom level by using bosonic Rb atoms [2,3], scientists have been able to observe the phase transitions of interacting quantum Ising spins [4], the dynamics of interacting quantum walkers [5], and magnon bound states [6]. Moreover, the measurement of entanglement entropy has also been realized [7]. Recently, detection technology has been expanded to fermionic Li [8,9] and K [10–12], culminating in the observation of a fermionic Mott insulator [13,14] and long-range antiferromagnetic ordering [15]. These experiments are significant toward the understanding of d-wave superconductivity. Improving the site-resolved imaging technology and extending it to new atomic species is an important step toward exploring a broader variety of strongly correlated phenomena. Among the candidates for extending this technology, highly dipolar atoms such as Dy and Er are promising for studying the extended Bose-Hubbard model and its underlying exotic phases of matter [16,17].

The most challenging task in the realization of site-resolved fluorescence imaging is fulfilling the requirement that atoms stay localized within a site while their fluorescence is collected. The conventional method for achieving this is to perform laser cooling simultaneously with imaging. Different cooling methods have been applied in the past experiments, including polarization gradient cooling in the case of Rb [1], Raman cooling for Li [8,9] and K [10], EIT cooling for K [11,12], and narrow-line optical molasses for Yb [18]. Although these cooling techniques have proven to be effective for imaging with a fidelity near unity, the experimental setups are complicated and often applicable only to a particular species.

A promising alternative to laser cooling-based systems is to use a sufficiently deep optical potential and short exposure time. This method was demonstrated using Yb atoms in [19], where an optical lattice nearly resonant with a transition from the excited state was used to create a large light shift. The required deep potential was created by coupling the ground and excited states with an excitation beam. The main advantage of this experimental setup is that it only requires a single

excitation beam and an available transition from the excited state and thus is readily extensible to new atomic species.

Prior to this research, access to strongly correlated quantum systems was limited to the systems based on laser cooling, and it was not clear whether the noncooled approach would provide sufficient fidelity to access the required physics. Here we report the direct observation of a Hubbard system using a noncooled site-resolved imaging device. We observe the shell structure of a bosonic ^{174}Yb Mott insulator with near unity fidelity, thus proving the effectiveness of this approach. We also go one step beyond the analysis in [19] by considering loss rates that are not constant and by estimating an upper limit for the hopping probability.

This paper is organized as follows. Section II briefly presents the experimental and imaging setup. Section III focuses upon the estimation of loss and hopping probability. In Sec. IV we fit the reconstructed atomic-density distributions to measure the temperatures of atoms in the insulator regime. Finally, in Sec. V we summarize and conclude our analysis.

II. EXPERIMENT

A. Preparation of the Mott insulator

We start our experiment by preparing a two-dimensional condensate of 5×10^4 bosonic ^{174}Yb that is positioned 2.6 μm below the surface of a solid immersion lens (SIL). The SIL enables us to increase the resolution of the imaging system and additionally fix the position of the atoms relative to its flat surface. The procedure to create and compress the condensate utilizes the "optical accordion" technique described in [19,20]. This technique comprises reflecting a laser beam from the flat substrate at a shallow angle to create a standing wave with tunable periodicity. In contrast to the procedure explained in [19], which utilizes a combination of two orthogonal optical accordions and one vertical optical dipole trap (ODT), here we opt to perform evaporative cooling using only one accordion beam and the vertical ODT (see Fig. 1). Both beams have a wavelength of 1080 nm and propagate in the $x + y = 0$ vertical plane. After compressing the condensate, we perform a second evaporative cooling by reducing the accordion beam power over 9 s. We control the number of atoms loaded into the two-dimensional optical lattice by adjusting the final power of the accordion beam.

To load the atoms into the two-dimensional optical lattice, we use an additional pair of beams (wavelength 1080 nm) propagating in the orthogonal $x = 0$ and $y = 0$ planes. The

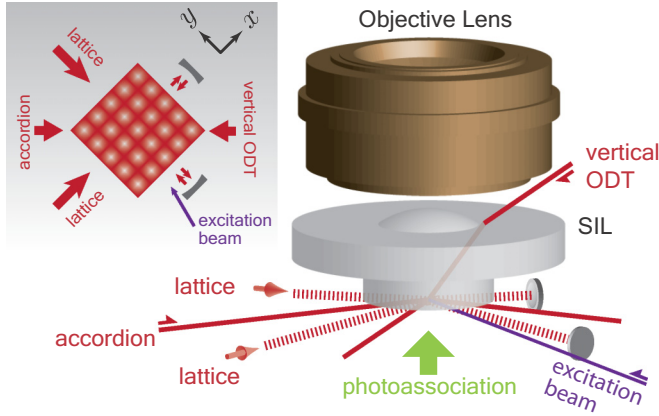―――――
*miranda.m.aa@m.titech.ac.jp

FIG. 1. Experimental setup. After creating a Bose-Einstein condensate and compressing it by using a combination of an optical accordion and a vertical ODT, a pair of retroreflected lattice beams is introduced to load the atoms into the two-dimensional optical lattice. The system is then driven into a Mott insulating state by gradually ramping up the intensity of the lattice beams. A photoassociation light is used to force inelastic light-assisted collisions on multiply occupied sites. Site-resolved imaging of the insulator is realized by irradiating a single excitation beam onto the atoms. No cooling mechanism is employed while the imaging system collects photons.

lattice beams are reflected from the SIL at the same angle as the optical accordion and retroreflected by using a concave mirror with a 50-mm radius of curvature. This creates a two-dimensional lattice with spacing $a_{\text{lat}} = 543.5$ nm in the x-y plane and a standing wave with 4.8 μm spacing in the z direction. The lattice beams have an elliptical cross section, with waists of 26 μm and 52 μm in the z and $x(y)$ directions, respectively. We load the atoms into the lattice by ramping up the potential depth to 6.5 E_r over 2 s while decreasing the intensity of the vertical and accordion beams. At this point, the atoms are in the superfluid regime, which we confirm by the presence of sharp interference peaks in the momentum distribution [21]. We further increase the lattice depth to 26 E_r over 1 s by using a smooth S-shaped curve to induce a phase transition into a Mott insulator.[1]

B. Site-resolved fluorescence imaging

We employ the photoassociation (PA) technique to remove pairs of atoms in multiply occupied sites and realize parity measurement of the number density [22,23]. The PA laser is red-detuned by 301 MHz from the $^1S_0 - {}^3P_1$ atomic transition at 556 nm. Pairs of atoms decay over 34(22) μs when an optical lattice depth of 1200 E_r and a PA laser beam intensity of 0.75 W/cm^2 is used. For this experiment, we ramp up the

---

[1]The superfluid-to-Mott-insulator transition is expected to occur at a lattice depth of 14 E_r. At the transition point, the tunneling rate is $J/h = 7.7$ Hz, the interaction energy is $U/k_B = 6.1$ nK, and the lattice transverse confinement is $\omega/2\pi = 35$ Hz. At 26 E_r the tunneling rate becomes negligible compared with the on-site interaction ($U/J \approx 240$) and fluctuations in the atom number are drastically reduced.
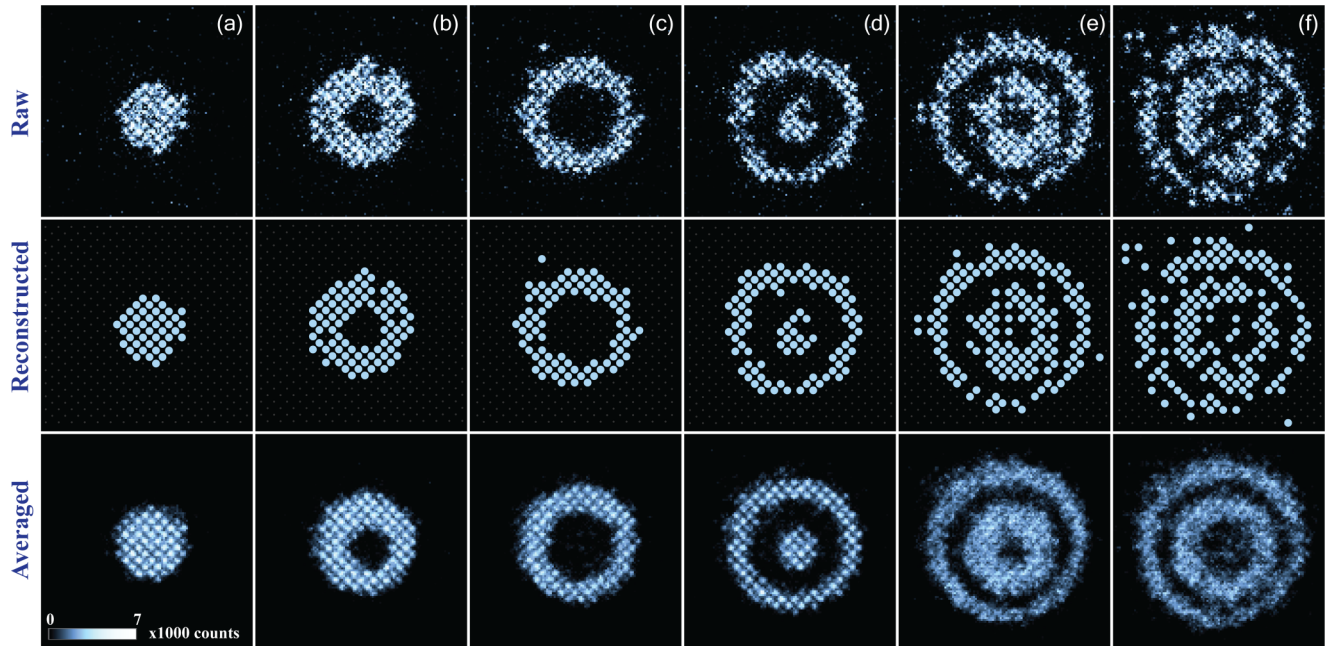
lattice depth in 10 ms and irradiate the PA beam for a period of 2 ms. This is expected to eliminate >99% of the atomic pairs while only producing an average of ∼0.5 photon scatterings in the rest of the atoms.

Finally, we obtain site-resolved imaging of a Mott insulator by further increasing the lattice depth to 3200 E_r over 5 ms, and irradiating an excitation beam (wavelength 399 nm, intensity 65 W/cm^2) upon the atoms for 40 μs. The scattered photons are collected by a high-resolution optical system (numerical aperture 0.81, magnification 110×) composed of the SIL and an objective lens and then focused into an emCCD camera (Andor iXon Ultra 888). The top row of Fig. 2 shows the obtained raw images for an increasing number of atoms in the trap. The observed concentric shells correspond to a fixed number of atoms in each shell, which is the characteristic structure of a Mott insulator under harmonic confinement [24,25]. To reconstruct the atomic-density distribution $n_{\text{det}}(\mathbf{r})$, we estimate the total fluorescence at each site by employing a computer algorithm based on deconvolution. The obtained total fluorescence is then compared with a previously determined fluorescence threshold to determine which site was occupied. The middle row in Fig. 2 shows the estimated density distribution corresponding to each of the images on top. Images in the bottom row are the result of averaging 10 fluorescence raw images.

III. FIDELITY

Here, we study the fidelity of the imaging system. In site-resolved imaging devices relying on cooling-based schemes to pin the atoms during the imaging process, the conventional method for estimating hopping and loss effects is to take two successive fluorescence images and compare their observed atomic-density distributions. As atoms are thermally in equilibrium during laser cooling, hopping and loss rates are constant. Thus, the comparison method provides a good estimation of both rates. In the case of the noncooled approach, the temperature of atoms during imaging is not constant but continuously increasing. This results in a number of trapped atoms that decays nonexponentially.

A. Loss effects

To estimate the loss effects, we obtain fluorescence images by employing the same procedure as in Fig. 2 but using a longer exposure time (300 μs instead of 40 μs). A typical observed image is shown in Fig. 3(b). Figure 3(a) shows the computed histogram for the number of sites as a function of the total fluorescence at each site. Note that the left peak of the histogram is determined by background noise on empty sites, which is caused by stray light from the excitation beam. From the histogram we compute the complementary cumulative distribution as shown in Fig. 3(c). For a large number of fluorescence counts, the background noise becomes negligible and the distribution is determined only by the fluorescence on occupied sites [circular points in Fig. 3(c)]. In accordance with the law of large numbers, the distribution of occupied sites is expected to be equivalent to the probability, $P_S(N_F)$, of an atom surviving after emitting N_F fluorescence counts, that is multiplied by the percentage of occupied sites.

FIG. 2. Site-resolved imaging of a bosonic ^{174}Yb Mott insulator. Top row corresponds to raw images obtained with the emCCD camera during an exposure time of $40\,\mu$s. The middle row shows the reconstructed atomic-density distribution obtained from the deconvolution algorithm. The estimated number of atoms in each image is (a) 45 ± 7, (b) 115 ± 5, (c) 179 ± 13, (d) 273 ± 12, (e) 486 ± 21, and (f) 592 ± 27. Bottom row shows the result of averaging 10 fluorescence raw images. Due to the presence of an external harmonic confinement in the optical lattices, the number of visible concentric Mott shells increases with the number of atoms.

In the case of a cooling-based scheme, $P_S(N_F)$ will decay exponentially as atoms have a constant temperature during imaging, resulting in a straight line on the semilog plot. In contrast, for the noncooled approach presented here, we observe a nonexponential decay. We fit the distribution of occupied sites with a known P_S obtained by simulation. This simulation considers losses due to heating and also light-induced excitations from the optical lattice [19]. From the fitting, we estimate that 21% of the sites are initially occupied. The solid line in Fig. 3(c) shows the fitting result. We find a remarkable agreement between the experimental data and the simulation, even at very large fluorescence counts. As a reference, we have also included the estimated curve for the histogram [solid line in Fig. 3(a)], which can be computed directly from P_S. We can then calculate the loss rate and percentage of lost atoms from the derivative and complement of P_S, respectively.

B. Hopping effects

Hopping effects are estimated using 100 images (exposure time $40\,\mu$s) of lattices with sparse and low populations, i.e., 2.6 atoms on an average [see Fig. 4(a)]. These samples are prepared by ramping down the lattice depth to $4\,E_r$ over 1 ms followed by a 0.5-s holding time. The shallow lattice depth allows atoms to disperse randomly along the lattice while the total number of atoms is reduced. The lattice depth is then ramped up to $26E_r$ over 10 ms to pin the positions of the atoms in the lattice and later imaged in the same way as the Mott insulator.

For each reconstructed image, we determine which sites are occupied or not by comparing the total fluorescence in

each site with an occupancy threshold. We then calculate the number of total occupied sites and the number of groups of two adjacent occupied sites in each image. Adjacent occupied sites are the result of either hopping events, a pair of atoms randomly occupying two adjacent sites,[2] or background events. For different choices of the occupancy threshold, the probability of finding two adjacent sites that are occupied then establishes an upper limit for the hopping probability, as shown in Fig. 4(c).

C. Loss and hopping probability

We set the occupancy threshold to 2×10^4 fluorescence counts. For this threshold, the loss and hopping probabilities are 1.8% and less than 0.7%, respectively. The low hopping probability is a characteristic of the noncooled imaging system, because atoms that become heated are rapidly accelerated by the radiative force exerted by the excitation beam and very rarely emit a sufficient number of photons in the neighboring sites for these sites to be considered as occupied.

IV. THERMOMETRY

Finally, we measure the temperature of the atomic cloud by analyzing the reconstructed density distribution. The Bose-Hubbard model describes the behavior of atoms trapped in a two-dimensional optical lattice with harmonic confinement. When the tunneling rate, J, is sufficiently smaller than the on-site interaction energy U ($U/J \gg 16.7$) [26], the number

---

[2]We estimate that the probability of finding two atoms occupying adjacent sites is 0.5% for a square lattice comprising 30×30 sites.
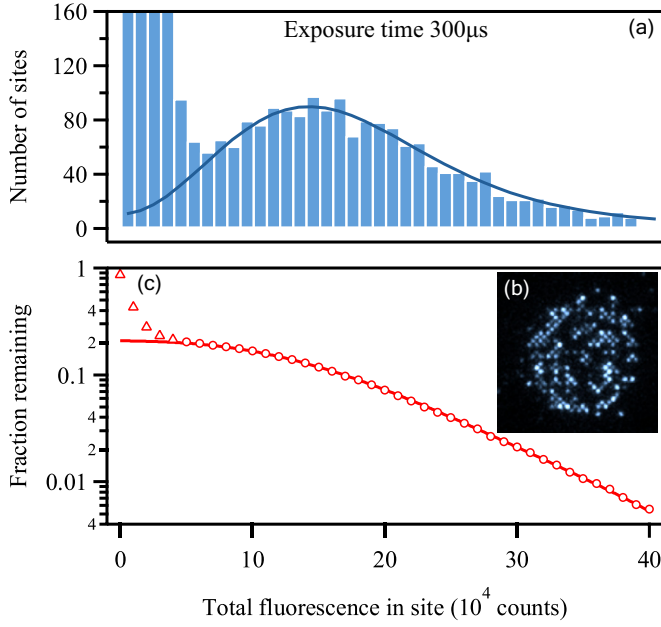
FIG. 3. Estimation of loss effects. (a) Histogram for the number of sites as a function of the total fluorescence at each site using 10 images taken at an exposure of 300 μs. The left peak corresponds to empty sites that are affected by stray background light. (b) Typical raw image. (c) Computed complementary cumulative function of the histogram, shown as a semilog plot. Circular points are fitted with a simulation (solid line) to obtain the percentage of occupied sites. Triangular points are not considered in the fitting because they include the contribution of empty sites.

FIG. 4. Estimation of hopping effects. (a) Typical raw image with a sparse population taken at an exposure time of 40 μs. (b) Histogram of the total fluorescence per site using 100 images containing an average of 2.6 atoms per image. Left and right peaks correspond to empty and occupied sites, respectively. (c) Upper limit of the hopping probability as a function of the occupancy threshold. Error bars denote 68% Clopper-Pearson confidence intervals.

density after parity projection, $n_{\text{det}}(\mathbf{r})$, is approximately (zero-tunneling approximation) [3]:

$$n_{\text{det}}(\mathbf{r}) = \frac{1}{Z} \sum_{n=1}^{\infty} \text{mod}_2(n) \exp\left[\frac{\mu(r)n - E_n}{k_B T}\right],$$

where Z is the grand canonical partition function, μ is the local chemical potential, T is the temperature, k_B is the Boltzmann constant, and $E_n = Un(n-1)/2$ is the interaction energy for a site occupied by n atoms. We apply the local density approximation $\mu = \mu_0 - 0.5m\omega^2 r^2$ where μ_0 is the global chemical potential and ω is the trap frequency of the harmonic confinement. Note that we consider an azimuthally symmetric function because we measured negligible ellipticity in our trap geometry.

We average the reconstructed number density azimuthally and then fit the result with the theoretical $n_{\text{det}}(\mathbf{r})$ (see Fig. 5), taking the loss effects into account. From the fitting, we extract the parameters μ_0/U and T/U, as well as the Mott shell radius $r_0 = \sqrt{2U/m\omega^2}$. This yields the parameters $T = 0.10(1)U/k_B$, $\mu_0 = 1.56(6)U$, $r_0 = 5.1(1)a_{\text{lat}}$ for (a), $T = 0.10(1)U/k_B$, $\mu_0 = 2.14(4)U$, $r_0 = 5.0(1)a_{\text{lat}}$ for (b), and $T = 0.21(2)U/k_B$, $\mu_0 = 3.38(7)U$, $r_0 = 5.0(1)a_{\text{lat}}$ for (c). From the extracted parameters we also calculate the entropy per atom resulting in $0.32(6)k_B$ for (a), $0.28(4)k_B$ for (b), and $0.34(3)k_B$ for (c).

The errors in the computed parameters are caused by the limited number of sites used in the azimuthal averages, which is reflected by the size of the error bars on the experimental
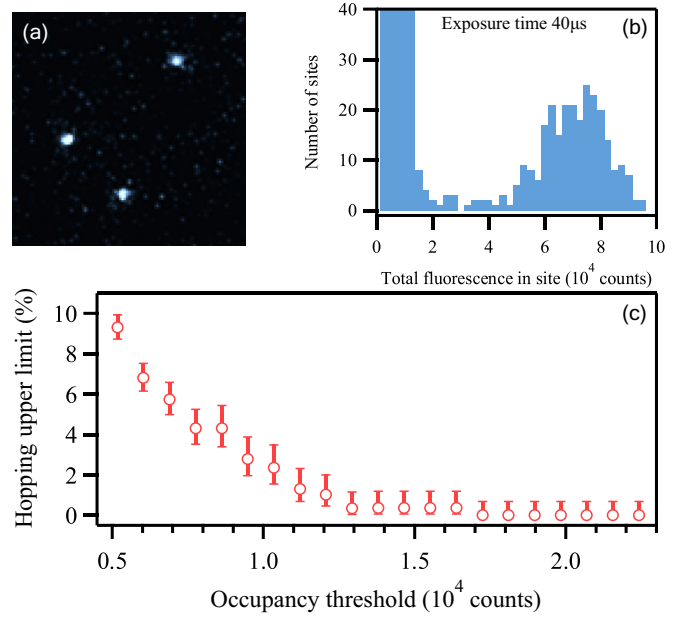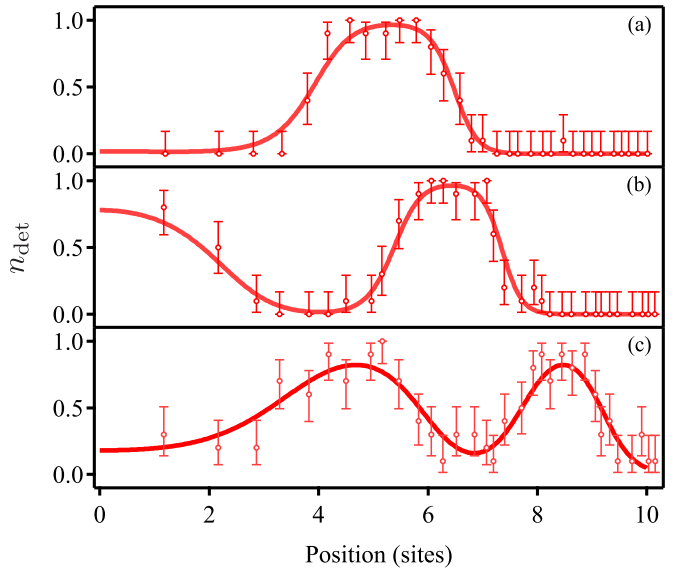

FIG. 5. Temperature measurement of a Mott insulator. The reconstructed atomic-density distribution is averaged azimuthally to obtain the radial profiles (points) and fitted using the grand-canonical ensemble described by the Bose-Hubbard model under the zero-tunneling approximation (solid lines). Error bars denotes 68% Clopper-Pearson confidence intervals. The experimental data for (a)–(c) correspond to the reconstructed density distributions in Figs. 2(c), 2(d) and 2(f), respectively. From each fitting, the global chemical potential μ_0, temperature T, and Mott radius r_0 are extracted.

data. Hopping effects are very small and produce a negligible error in the measurement. Increasing the accuracy of this thermometer would require the use of traps having smaller ω or increasing U by using larger s-wave scattering lengths.

V. CONCLUSIONS

In conclusion, we have demonstrated the site-resolved observation of a Mott insulator by using a noncooled method. This approach is robust against mechanical instabilities in the optical system owing to the short exposure time used during imaging. The simplicity of the setup that uses only one excitation beam that does not require retroreflection makes it readily applicable to other species. In particular, lanthanoid atoms benefit from the noncooled method as they have a large mass, which results in small recoil energies ensuring small

losses. We have also presented a method for estimating the loss and hopping effects and found that our system has comparable fidelity to that of its laser cooling-based counterparts. Our results are promising for the study of the Fermi-Hubbard model using a Yb gas in its generalized SU(N) form [27,28].

[1] W. S. Bakr, J. I. Gillen, A. Peng, S. Folling, and M. Greiner, Nature (London) **462**, 74 (2009).

[2] W. S. Bakr, A. Peng, M. E. Tai, R. Ma, J. Simon, J. I. Gillen, S. Fölling, L. Pollet, and M. Greiner, Science **329**, 547 (2010).

[3] J. F. Sherson, C. Weitenberg, M. Endres, M. Cheneau, I. Bloch, and S. Kuhr, Nature (London) **467**, 68 (2010).

[4] J. Simon, W. S. Bakr, R. Ma, M. E. Tai, P. M. Preiss, and M. Greiner, Nature (London) **472**, 307 (2011).

[5] P. M. Preiss, R. Ma, M. E. Tai, A. Lukin, M. Rispoli, P. Zupancic, Y. Lahini, R. Islam, and M. Greiner, Science **347**, 1229 (2015).

[6] T. Fukuhara, P. Schausz, M. Endres, S. Hild, M. Cheneau, I. Bloch, and C. Gross, Nature (London) **502**, 76 (2013).

[7] R. Islam, R. Ma, P. M. Preiss, M. Eric Tai, A. Lukin, M. Rispoli, and M. Greiner, Nature (London) **528**, 77 (2015).

[8] M. F. Parsons, F. Huber, A. Mazurenko, C. S. Chiu, W. Setiawan, K. Wooley-Brown, S. Blatt, and M. Greiner, Phys. Rev. Lett. **114**, 213002 (2015).

[9] A. Omran, M. Boll, T. A. Hilker, K. Kleinlein, G. Salomon, I. Bloch, and C. Gross, Phys. Rev. Lett. **115**, 263001 (2015).

[10] L. W. Cheuk, M. A. Nichols, M. Okan, T. Gersdorf, V. V. Ramasesh, W. S. Bakr, T. Lompe, and M. W. Zwierlein, Phys. Rev. Lett. **114**, 193001 (2015).

[11] E. Haller, J. Hudson, A. Kelly, D. A. Cotta, B. Peaudecerf, G. D. Bruce, and S. Kuhr, Nat. Phys. **11**, 738 (2015).

[12] G. J. A. Edge, R. Anderson, D. Jervis, D. C. McKay, R. Day, S. Trotzky, and J. H. Thywissen, Phys. Rev. A **92**, 063406 (2015).

[13] D. Greif, M. F. Parsons, A. Mazurenko, C. S. Chiu, S. Blatt, F. Huber, G. Ji, and M. Greiner, Science **351**, 953 (2016).

[14] L. W. Cheuk, M. A. Nichols, K. R. Lawrence, M. Okan, H. Zhang, and M. W. Zwierlein, Phys. Rev. Lett. **116**, 235301 (2016).

[15] A. Mazurenko, C. S. Chiu, G. Ji, M. F. Parsons, M. Kanász-Nagy, R. Schmidt, F. Grusdt, E. Demler, D. Greif, and M. Greiner, Nature (London) **545**, 462 (2017).

[16] D. Rossini and R. Fazio, New J. Phys. **14**, 065012 (2012).

[17] S. Baier, M. J. Mark, D. Petter, K. Aikawa, L. Chomaz, Z. Cai, M. Baranov, P. Zoller, and F. Ferlaino, Science **352**, 201 (2016).

[18] R. Yamamoto, J. Kobayashi, T. Kuno, K. Kato, and Y. Takahashi, New J. Phys. **18**, 023016 (2016).

[19] M. Miranda, R. Inoue, Y. Okuyama, A. Nakamoto, and M. Kozuma, Phys. Rev. A **91**, 063414 (2015).

[20] M. Miranda, A. Nakamoto, Y. Okuyama, A. Noguchi, M. Ueda, and M. Kozuma, Phys. Rev. A **86**, 063615 (2012).

[21] M. Greiner, O. Mandel, T. Esslinger, T. W. Hansch, and I. Bloch, Nature (London) **415**, 39 (2002).

[22] S. Tojo, M. Kitagawa, K. Enomoto, Y. Kato, Y. Takasu, M. Kumakura, and Y. Takahashi, Phys. Rev. Lett. **96**, 153201 (2006).

[23] S. Sugawa, K. Inaba, S. Taie, R. Yamazaki, M. Yamashita, and Y. Takahashi, Nat. Phys. **7**, 642 (2011).

[24] B. DeMarco, C. Lannert, S. Vishveshwara, and T.-C. Wei, Phys. Rev. A **71**, 063601 (2005).

[25] S. Fölling, A. Widera, T. Müller, F. Gerbier, and I. Bloch, Phys. Rev. Lett. **97**, 060403 (2006).

[26] S. Wessel, F. Alet, M. Troyer, and G. G. Batrouni, Phys. Rev. A **70**, 053615 (2004).

[27] C. Hofrichter, L. Riegger, F. Scazza, M. Höfer, D. R. Fernandes, I. Bloch, and S. Fölling, Phys. Rev. X **6**, 021030 (2016).

[28] C. Honerkamp and W. Hofstetter, Phys. Rev. Lett. **92**, 170403 (2004).